Field Oriented Modeling and Control of Six Phase, Open-Delta Winding, Interior Permanent Magnet Synchronous Machines considering Current Unbalance and Zero Sequence Currents

Murat Senol, Michael Schubert,
Georges Engelmann and Rik W. De Doncker
Institute for Power Electronics and Electrical Drives (ISEA)
RWTH Aachen University, Germany
e-mail: post@isea.rwth-aachen.de

Thorben Grosse and Kay Hameyer
Institute of Electrical Machines (IEM)
RWTH Aachen University, Aachen, Germany
e-mail: post@iem.rwth-aachen.de

***Abstract*—Industrial and academic interest on multiphase electric machines have been steadily increasing due to the advantages they provide compared to their three phase counterparts. They offer higher efficiency and better fault tolerance. The power is distributed across a larger number of machine phases and inverter legs, which allows the use of semiconductor devices with lower ratings. These advantages are especially benecifial for electric and hybrid vehicle applications.**

Increasing the battery pack voltage of an electric vehicle increases the cost and complexity, while decreasing the energy density of the battery pack. Therefore, electric vehicle system design may benefit on the vehicle level from a more complex drivetrain with higher dc link voltage utilization. H bridge inverters as well as multiphase machines provide increased dc-link voltage utilization compared to three phase inverters and machines.

A low voltage, high power drivetrain is designed for an electric vehicle using an asymmetrical six phase, open-delta interior permanent magnet synchronous machine (IPMSM) and an H Bridge inverter. Field oriented modeling and control of such a system is investigated in this paper. The sources of unbalance and zero sequence current components are explored.

***Keywords*—Field oriented control, multiphase machines, asymmetrical six phase, open delta, H Bridge inverter, zero sequence current, resonant controller**

I. Introduction

Multiphase machine drives provide reduced phase current ratings, increased dc-link utilization, lower dc link current harmonics, higher efficiency, improved fault tolerance, decreased torque ripples, and higher reliability compared to three phase drive systems. Therefore, they are increasingly employed in electric and hybrid electric vehicles, ship propulsion, locomotive traction, aircrafts, and wind power generation.

A large variety of control strategies has been proposed to control six phase machines. Direct torque control (DTC) has low machine parameter dependence and fast dynamic torque response. Predictive control provides similar dynamic torque response as DTC. However, the high computational effort limits its application. Vector control has the advantage of simplicity, while it is limited in dynamic response by the small bandwidth of the PI controllers. An extensive literature survey about these control methods can be found in [5].

A comprehensive analysis of the machine properties of a six phase IPMSM is presented in this paper to provide insight into the machine-based disturbances which affect the control of six phase open-delta winding machines. This information is used to suggest an accurate and fast machine model which can be used in control simulations of such machines. The control method, which has been presented in [5] for dual three phase, surface-mounted PMSMs, is extended to control six phase, open-delta winding IPMSMs. Simulation results are compared to measurements to verify the validity of the model, and efficiency measurements are provided.

II. Field Oriented Modeling

In conventional rotor field oriented control, the machine phase variables (current, voltage and flux linkage) are transformed into a two phase orthogonal system which is aligned with the rotor flux linkage. The current component on the direct axis i_d influences the stator flux linkage, while the current component on the quadrature axis i_q produces torque. Therefore, the flux generating and torque generating current components are decoupled and can be controlled with simpler controllers. [1]

Conventionally, two PI controllers are used to control i_d and i_q, as illustrated by the signal flow diagram in Fig. 1. The controller receives information about torque demand T_m^* and maximum allowed stator voltage $u_\mathrm{s}^\mathrm{max}$. Rotor position and speed are calculated using position sensor data. The data is processed (usually using look-up tables) to obtain reference values $i_\mathrm{s.d}^*$ and $i_\mathrm{s.q}^*$. The transformed phase currents are fed back to the PI controllers, which calculate the set voltages u_d^* and u_q^* that should be applied to the machine. These values are then transformed back to the three phase system and applied to the machine through the inverter.

978-1-4673-9550-2/16/$31.00 ©2016 IEEE

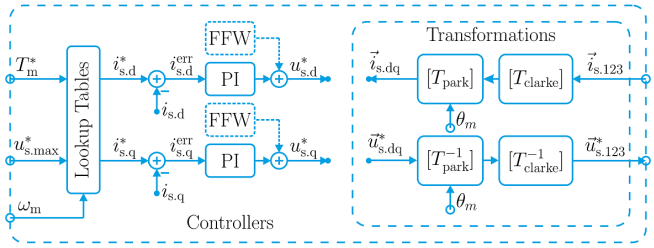

Fig. 1. Control diagram of conventional field oriented control

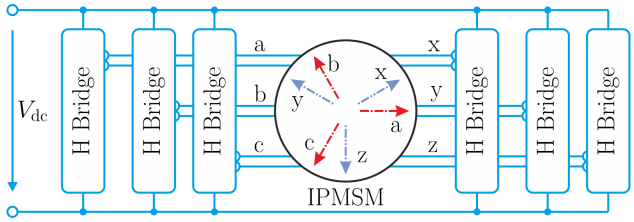

Fig. 2. Six phase open-delta drivetrain topology

A. Field Oriented Transformations

The six phase, open-delta machine can be considered as two three-phase machines with a stator phase shift of $\theta_{\mathrm{s}} = 30°$ in the same stator core, as shown in Fig. 2. To achieve full control of torque and flux linkage, as well as phase currents; a six phase to six orthogonal phase field oriented transformation set is required, as given in (1)–(3). $\vec{F}$ can be current, voltage, or flux linkage vectors in different vector spaces. $\vec{F}_{\mathrm{az}}$ represents the vectors in the phase space, $\vec{F}_{\alpha\beta}$ represents the vectors in the stator oriented orthogonal space, and $\vec{F}_{\mathrm{dq}}$ represents the vectors in the rotor field oriented orthogonal space. These vectors are given explicitly in (4)–(6).

$$\begin{bmatrix} \vec{F}_{\alpha\beta} \end{bmatrix} = \begin{bmatrix} T_{\mathrm{clarke}} \end{bmatrix} \cdot \begin{bmatrix} \vec{F}_{\mathrm{az}} \end{bmatrix} \tag{1}$$

$$\begin{bmatrix} \vec{F}_{\mathrm{dq}} \end{bmatrix} = \begin{bmatrix} T_{\mathrm{park}} \end{bmatrix} \cdot \begin{bmatrix} \vec{F}_{\alpha\beta} \end{bmatrix} \tag{2}$$

$$\begin{bmatrix} \vec{F}_{\mathrm{az}} \end{bmatrix} = \begin{bmatrix} T^{-1}_{\mathrm{clarke}} \end{bmatrix} \cdot \begin{bmatrix} T^{-1}_{\mathrm{park}} \end{bmatrix} \cdot \begin{bmatrix} \vec{F}_{\mathrm{dq}} \end{bmatrix} \tag{3}$$

$$\begin{bmatrix} \vec{F}_{\mathrm{az}} \end{bmatrix} = \begin{bmatrix} F_{\mathrm{a}} & F_{\mathrm{x}} & F_{\mathrm{b}} & F_{\mathrm{y}} & F_{\mathrm{c}} & F_{\mathrm{z}} \end{bmatrix}^T \tag{4}$$

$$\begin{bmatrix} \vec{F}_{\alpha\beta} \end{bmatrix} = \begin{bmatrix} F_{\alpha} & F_{\beta} & F_{\mathrm{z1}} & F_{\mathrm{z2}} & F_{\mathrm{o1}} & F_{\mathrm{o2}} \end{bmatrix}^T \tag{5}$$

$$\begin{bmatrix} \vec{F}_{\mathrm{dq}} \end{bmatrix} = \begin{bmatrix} F_{\mathrm{d}} & F_{\mathrm{q}} & F_{\mathrm{zd}} & F_{\mathrm{zq}} & F_{\mathrm{o1}} & F_{\mathrm{o2}} \end{bmatrix}^T \tag{6}$$

The power invariant Clarke transformation $[T_{\mathrm{clarke}}]$, given in (11), is constructed considering the harmonic components in the machine variables. This transformation maps the fundamental and $(12k \pm 1)^{th}$ harmonics to the $\alpha\beta$ plane, $(12k - 6 \pm 1)^{th}$harmonics to the z_{12} plane, and $(6k - 3)^{rd}$ harmonics to the o_{12} plane, where $k \in \{1, 2, 3, ...\}$. [4]

It should be noted that the z_{12} plane also represents the unbalance between the variables of two machine sets abc and xyz in $\alpha\beta$ plane while the o_{12} plane represents the zero sequence variables of each of these machine sets, as shown in (7)–(10).

$$F_{\mathrm{z1}} = F_{\alpha_{\mathrm{abc}}} - F_{\alpha_{\mathrm{xyz}}} \tag{7}$$

$$F_{\mathrm{z2}} = F_{\beta_{\mathrm{xyz}}} - F_{\beta_{\mathrm{abc}}} \tag{8}$$

$$F_{\mathrm{o1}} = \sqrt{2/6} \cdot (F_a + F_b + F_c) \tag{9}$$

$$F_{\mathrm{o2}} = \sqrt{2/6} \cdot (F_x + F_y + F_z) \tag{10}$$

The Park transformation $[T_{\mathrm{park}}]$, given in (12), rotates the vectors on $\alpha\beta$ plane to rotor field oriented dq plane. It also rotates the vectors in z_{12} plane to z_{dq} plane such that the z_{dq} plane vectors represents the unbalance between the variables of the two machine sets abc and xyz in dq plane.

It is explained in detail in [5], how the 5^{th} and 7^{th} harmonics in z_{12} plane are converted to 6^{th} harmonics in z_{dq} plane through the Park transformation. Similarly, the 11^{th} and 13^{th} harmonics in $\alpha\beta$ plane are converted to 12^{th} harmonics in dq plane.

The Clarke and inverse Clarke transformations can be calculated and stored numerically instead of variables, for example using matlab, since all elements are constants. For inverse Park transformation, Park transformation can be used with $-\theta_{\mathrm{m}}$ since it is only a rotating transformation.

B. Simplified Machine Model

The stator voltage equation of a six phase, open-delta, interior permanent magnet machine is given in (13). This equation holds for both phase space variables and stator oriented orthogonal space variables, since the Clarke transformation is time and position invariant.

In the following equations, $\vec{u}_{\mathrm{s}}$ is the stator voltage, $\vec{i}_{\mathrm{s}}$ is the stator current, $\vec{\psi}_{\mathrm{s}}$ is the stator flux linkage, $\vec{\psi}_{\mathrm{f}}$ is the magnet flux linkage, $[R_{\mathrm{s}}]$ is the 6×6 diagonal stator resistance matrix, and $[L_{\mathrm{s}}]$ is the stator inductance matrix. The Park transformation is applied to (13) to obtain (14). [1]

$$\vec{u}_{\mathrm{s}.\alpha\beta} = [R_{\mathrm{s}}]\, \vec{i}_{\mathrm{s}.\alpha\beta} + \frac{\mathrm{d}}{\mathrm{d}t}\, \vec{\psi}_{\mathrm{s}.\alpha\beta} \tag{13}$$

$$\begin{bmatrix} u_{\mathrm{s.d}} \\ u_{\mathrm{s.q}} \\ u_{\mathrm{s.zd}} \\ u_{\mathrm{s.zq}} \\ u_{\mathrm{s.o1}} \\ u_{\mathrm{s.o2}} \end{bmatrix} = \begin{bmatrix} R_{\mathrm{s}} i_{\mathrm{s.d}} \\ R_{\mathrm{s}} i_{\mathrm{s.q}} \\ R_{\mathrm{s}} i_{\mathrm{s.zd}} \\ R_{\mathrm{s}} i_{\mathrm{s.zq}} \\ R_{\mathrm{s}} i_{\mathrm{s.o1}} \\ R_{\mathrm{s}} i_{\mathrm{s.o2}} \end{bmatrix} + \frac{\mathrm{d}}{\mathrm{d}t} \begin{bmatrix} \psi_{\mathrm{s.d}} \\ \psi_{\mathrm{s.q}} \\ \psi_{\mathrm{s.zd}} \\ \psi_{\mathrm{s.zq}} \\ \psi_{\mathrm{s.o1}} \\ \psi_{\mathrm{s.o2}} \end{bmatrix} + \begin{bmatrix} -\omega_{\mathrm{m}} \psi_{\mathrm{s.q}} \\ \omega_{\mathrm{m}} \psi_{\mathrm{s.d}} \\ -\omega_{\mathrm{m}} \psi_{\mathrm{s.zq}} \\ \omega_{\mathrm{m}} \psi_{\mathrm{s.zd}} \\ 0 \\ 0 \end{bmatrix} \tag{14}$$

A simplified machine model can be obtained assuming that the machine has sinusoidal back EMF, no iron losses, no mutual leakage inductance, no asymmetries, and no saturation. Considering the assumptions above, it can be further assumed that $\vec{\psi}_{\mathrm{f.dq}}$ is a 6 dimensional zero vector with the exception of $\psi_{\mathrm{f.d}} = \psi_{\mathrm{f}}$, $[R_{\mathrm{s}}]$ is a 6×6 diagonal matrix with R_{s} as all non-zero elements, and $[L_{\mathrm{s.dq}}]$ is a 6×6 diagonal matrix of constant elements, i.e. independent of rotor position and stator currents.

$$\vec{\psi}_{\mathrm{s.dq}} = [L_{\mathrm{s.dq}}]\, \vec{i}_{\mathrm{s.dq}} + \vec{\psi}_{\mathrm{f.dq}} \tag{15}$$

$$\frac{\mathrm{d}}{\mathrm{d}t}\, \vec{\psi}_{\mathrm{s.dq}} = [L_{\mathrm{s.dq}}]\, \frac{\mathrm{d}}{\mathrm{d}t}\, \vec{i}_{\mathrm{s.dq}} + \frac{\mathrm{d}}{\mathrm{d}t}\, \vec{\psi}_{\mathrm{f.dq}} \tag{16}$$

$$[\ T_{\mathrm{clarke}}\ ] = \sqrt{\frac{2}{6}} \cdot \begin{bmatrix} 1 & \cos(\theta_\mathrm{s}) & \cos(4\theta_\mathrm{s}) & \cos(5\theta_\mathrm{s}) & \cos(8\theta_\mathrm{s}) & \cos(9\theta_\mathrm{s}) \\ 0 & \sin(\theta_\mathrm{s}) & \sin(4\theta_\mathrm{s}) & \sin(5\theta_\mathrm{s}) & \sin(8\theta_\mathrm{s}) & \sin(9\theta_\mathrm{s}) \\ 1 & \cos(5\theta_\mathrm{s}) & \cos(8\theta_\mathrm{s}) & \cos(\theta_\mathrm{s}) & \cos(4\theta_\mathrm{s}) & \cos(9\theta_\mathrm{s}) \\ 0 & \sin(5\theta_\mathrm{s}) & \sin(8\theta_\mathrm{s}) & \sin(\theta_\mathrm{s}) & \sin(4\theta_\mathrm{s}) & \sin(9\theta_\mathrm{s}) \\ 1 & 0 & 1 & 0 & 1 & 0 \\ 0 & 1 & 0 & 1 & 0 & 1 \end{bmatrix} \tag{11}$$

$$[\ T_{\mathrm{park}}\ ] = \begin{bmatrix} \cos(\theta_\mathrm{m}) & \sin(\theta_\mathrm{m}) & 0 & 0 & 0 & 0 \\ -\sin(\theta_\mathrm{m}) & \cos(\theta_\mathrm{m}) & 0 & 0 & 0 & 0 \\ 0 & 0 & \cos(\theta_\mathrm{m}) & \sin(\theta_\mathrm{m}) & 0 & 0 \\ 0 & 0 & -\sin(\theta_\mathrm{m}) & \cos(\theta_\mathrm{m}) & 0 & 0 \\ 0 & 0 & 0 & 0 & 1 & 0 \\ 0 & 0 & 0 & 0 & 0 & 1 \end{bmatrix} \tag{12}$$

The simplified equivalent circuit of the machine, given in Fig. 3, has no disturbances in the $\mathrm{z_{dq}}$ and $\mathrm{o_{12}}$ planes. It can be used for educational purposes or to observe the isolated effect of the inverter non-idealities on the control. However, it does not sufficiently represent the machine in real life to simulate and investigate a control method. In fact, in this model, the $\mathrm{z_{dq}}$ and $\mathrm{o_{12}}$ plane currents can be adjusted to zero, simply by setting the voltages to zero.

C. Non-Ideal Properties of the Machine

The effects of current and rotor position dependencies of stator inductances and the magnet flux linkages should be investigated to obtain a more accurate machine model. A set of look-up tables has been created using FEM analysis for this purpose; which provides the stator and magnet flux linkage vectors $\vec{\psi}_{\mathrm{s.az}}$ and $\vec{\psi}_{\mathrm{f.az}}$, the stator inductance matrix $[L_{\mathrm{s.az}}]$, and torque for changing rotor position θ_m, and stator currents $i_{\mathrm{s.d}}$ and $i_{\mathrm{s.q}}$.

The model can be further improved in precision by adding new dimensions of current dependencies for $\mathrm{z_{dq}}$ and $\mathrm{o_{12}}$ plane current components. However, this increases the simulation times significantly, both for the FEM analysis and the control simulations where these tables are used. An adequate control that can keep these current components close to zero renders this effort futile in the first place.

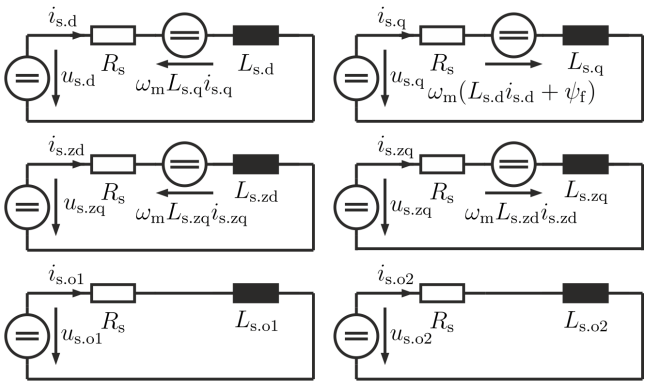

Fig. 3. Simplified equivalent circuit of the machine

1) Stator Current and Rotor Position Dependency of Magnet Flux Linkages:

The magnet flux linkages in each orthogonal dimension as a function of rotor position for different stator currents are given in Fig. 4. The instantaneous values of these flux linkages multiplied by the rotor speed ω_m appear as back EMF within dq and $\mathrm{z_{dq}}$ planes, while the derivatives of these components appear as harmonic back EMF in all dimensions of the equivalent circuit.

It can be noted that there are mainly dc components and 12^{th} harmonics in dq plane magnet flux linkages, while there are essentially only 6^{th} harmonics in $\mathrm{z_{dq}}$ plane. The $\mathrm{o_{12}}$ plane is dominated by 3^{rd} and 9^{th} harmonics.

The transformations in this study have been carried out assuming the magnet flux linkage, i.e. rotor flux linkage, has a constant position on the rotor. Consequently, the rotor position θ_m is used for Park transformations instead of the exact position of rotor flux linkage. The error in this assumption manifests as a dc component in magnet flux linkage $\psi_{\mathrm{f.q}}$ when the stator currents increase due to saturation. The magnet flux linkage deviates about 6° in the worst case.

However, since the machine is an IPMSM, $i_{\mathrm{s.d}} = 0$ control is not employed. Instead, either FEM analysis or measurements are employed to create lookup tables to determine dq current trajectories for torque demand and speed. If rotor position oriented transformations are used throughout this whole process, there will not be any performance degradation.

This issue of changing magnet flux linkage vector position compared to rotor position can also be handled by calculating this deviation as a function of stator currents. It should be noted, however, that this effort will not bring any additional benefits compared to using rotor position and using rotor position oriented lookup tables.

2) Stator Current and Rotor Position Dependency and Non-diagonality of Transformed Inductances:

The transformed stator inductance matrix is easily taken out of the derivative in (16), since it is assumed to be a 6×6 diagonal matrix of constant elements. However, the FEM analysis shows the strong dependence of $[L_{\mathrm{s.dq}}]$ on stator currents as well as rotor position, as shown in Fig. 5.

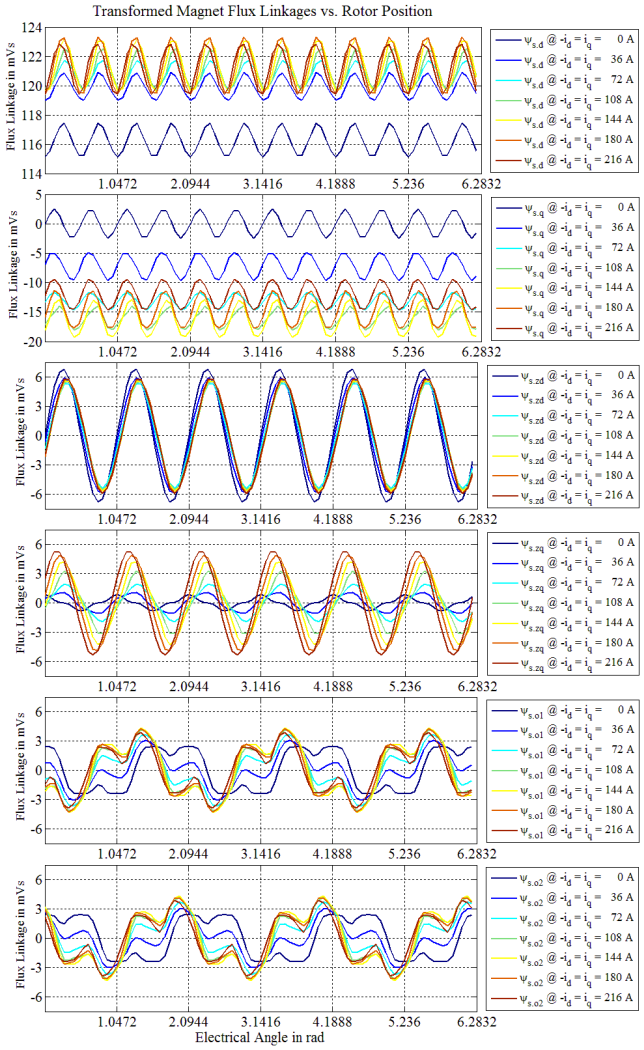

Fig. 4. Magnet flux linkages calculated by FEM analysis

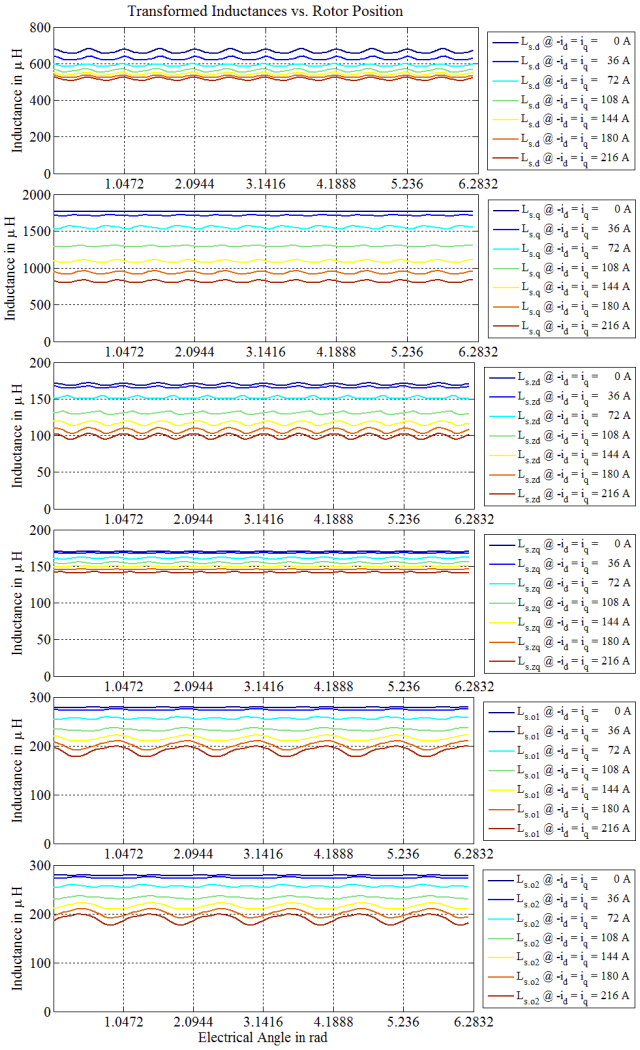

Fig. 5. Transformed self inductances calculated by FEM analysis

Therefore, the stator flux linkage derivative term in (14) takes the more complicated form given in (17) and (18). The first term in (18) is the instantaneous inductance, the second term is saturation, and the last term is the back EMF, induced by the rotor position dependent inductance change.

$$\frac{\mathrm{d}}{\mathrm{d}t}\,\vec{\psi}_{\mathrm{s.dq}} = \frac{\mathrm{d}}{\mathrm{d}t}\,\left[L_{\mathrm{s.dq}}(\vec{i}_{\mathrm{s.dq}},\theta_{\mathrm{m}})\right]\vec{i}_{\mathrm{s.dq}} + \frac{\mathrm{d}}{\mathrm{d}t}\,\vec{\psi}_{\mathrm{f.dq}} \tag{17}$$

$$\begin{aligned}\frac{\mathrm{d}\left[L_{\mathrm{s.dq}}(\vec{i}_{\mathrm{s.dq}},\theta_{\mathrm{m}})\right]\vec{i}_{\mathrm{s.dq}}(t)}{\mathrm{d}t} = \\ \left[L_{\mathrm{s.dq}}(\vec{i}_{\mathrm{s.dq}},\theta_{\mathrm{m}})\right]\,\frac{\mathrm{d}\,\vec{i}_{\mathrm{s.dq}}(t)}{\mathrm{d}t} + \\ \vec{i}_{\mathrm{s.dq}}(t)\,\frac{\partial\left[L_{\mathrm{s.dq}}(\vec{i}_{\mathrm{s.dq}},\theta_{\mathrm{m}})\right]}{\partial\vec{i}_{\mathrm{s.dq}}}\,\frac{\mathrm{d}\,\vec{i}_{\mathrm{s.dq}}(t)}{\mathrm{d}t} + \\ \vec{i}_{\mathrm{s.dq}}(t)\,\frac{\partial\left[L_{\mathrm{s.dq}}(\vec{i}_{\mathrm{s.dq}},\theta_{\mathrm{m}})\right]}{\partial\theta_{\mathrm{m}}}\,\frac{\mathrm{d}\,\theta_{\mathrm{m}}(t)}{\mathrm{d}t}\end{aligned} \tag{18}$$

The FEM analysis results also indicate that the inductance matrix $\left[L_{\mathrm{s.dq}}(\vec{i}_{\mathrm{s.dq}},\theta_{\mathrm{m}})\right]$ is not diagonal, which implies that there is inductive coupling between the orthogonal planes. This coupling also has a significant impact on the machine behaviour and will be shown that it cannot be neglected.

The equivalent circuit model of the machine turns out to be very complex once the non-ideal properties of the machine are also included in the model, especially when the couplings between the supposedly orthogonal dimensions are taken into account. Therefore, the rotor field oriented machine model with an ideal rotating transformer (IRTF) is recommended to model the machine [1].

D. Field Oriented Machine Model

The field oriented machine model with an ideal rotating transformer (IRTF) focuses on the flux linkages in the machine. Since the calculation of the derivative of stator flux linkage is avoided, the model is significantly easier to understand and implement.

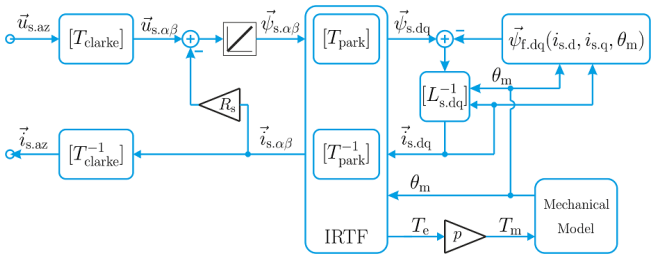

Fig. 6. IRTF based machine model

The machine model receives the phase voltage information $\vec{u}_{\mathrm{s.az}}$ as input. This vector is transformed using the Clarke transformation to obtain the voltage vector in stator oriented orthogonal space $\vec{u}_{\mathrm{s.}\alpha\beta}$. Once the resistive voltage drop is substracted from $\vec{u}_{\mathrm{s.}\alpha\beta}$, the remaining voltage is integrated to calculate the stator flux linkage vector in stator oriented orthogonal space $\vec{\psi}_{\mathrm{s.}\alpha\beta}$, according to (13).

Rotor field oriented flux linkage vector $\vec{\psi}_{\mathrm{s.dq}}$ can then be calculated by rotating $\vec{\psi}_{\mathrm{s.}\alpha\beta}$ using the Park transformation. The current vector in this vector space $\vec{i}_{\mathrm{s.dq}}$ can be calculated by subtracting the magnet flux linkage $\vec{\psi}_{\mathrm{f.dq}}$ from the stator flux linkage $\vec{\psi}_{\mathrm{s.dq}}$ and multiplying the result with the inverse inductance matrix $\left[L^{-1}_{\mathrm{s.dq}}\right]$, as in (15).

The phase current vector $\vec{i}_{\mathrm{s.az}}$ can finally be calculated by using the inverse Park and inverse Clarke transformations on the rotor field oriented current vector $\vec{i}_{\mathrm{s.dq}}$, according to (3).

The mechanical torque T_{e} produced by the machine can be calculated as the magnitude of the cross product of stator flux linkage vector $\vec{\psi}_{\mathrm{s.}\alpha\beta}$ and stator current vector $\vec{i}_{\mathrm{s.}\alpha\beta}$ multiplied by the pole pair number p. Since the contributions of the other planes are negligibly small, the equation can be simplified to include only the cross product in dq plane, as in (19).

$$T_{\mathrm{m}} = p \cdot T_{\mathrm{e}} = p \cdot (\psi_{\mathrm{s.d}} i_{\mathrm{s.q}} - \psi_{\mathrm{s.q}} i_{\mathrm{s.d}}) \tag{19}$$

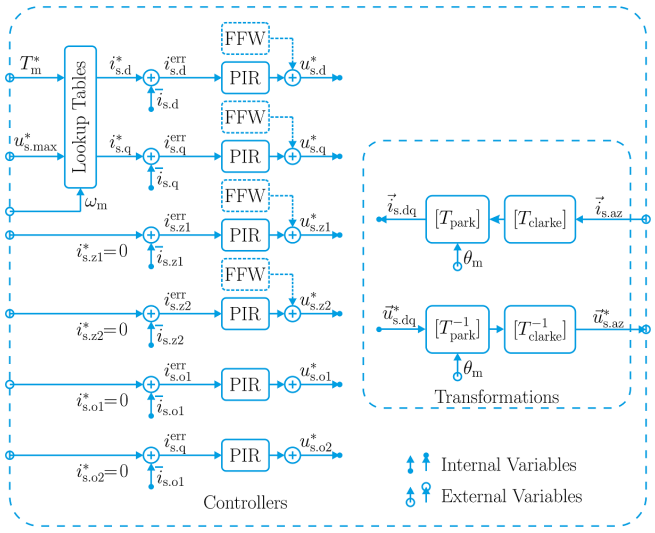

Fig. 7. Control diagram of a six phase, open-delta IPMSM drivetrain

It is very important to note that $\vec{\psi}_{\mathrm{f.dq}}$ and $\left[L^{-1}_{\mathrm{s.dq}}\right]$ are strongly dependent on the rotor position θ_{m} and the stator currents $i_{\mathrm{s.d}}$ and $i_{\mathrm{s.q}}$. A machine model that neglects these dependencies is likely not to properly represent the machine in real life.

III. Field Oriented Control

The rotor field oriented control of six phase, open delta IPMSM is carried out similarly to the conventional field oriented control. Six current controllers are employed for each dimension of the rotor field oriented orthogonal space vector of current $\vec{i}_{\mathrm{s.dq}}$. The set values of the current components in dq plane $i^*_{\mathrm{s.d}}$ and $i^*_{\mathrm{s.q}}$ are calculated using lookup tables, which are created either by using FEM analysis or measurements. Since the current components in $\mathrm{z_{dq}}$ plane and $\mathrm{o_{12}}$ plane do not contribute to the electromechanical energy conversion, the set values of these current components, $i^*_{\mathrm{s.zd}}$, $i^*_{\mathrm{s.zq}}$, $i^*_{\mathrm{s.o1}}$ and $i^*_{\mathrm{s.o2}}$ are always zero.

The field oriented control diagram is given in Fig. 7, where PIR denotes modified proportional integral resonant controllers, which are explained in detail below,. The optional feed forward components (FFW), which are not explored further in this paper, can be used to improve the dynamic performance of the control.

A. Proportional Integral Resonant Controllers

PI controllers are not well suited to following alternating references or eliminating alternating errors due to their limited bandwidth. Different kinds of proportional resonant controllers have been proposed to address this control issue. Modified proportional integral resonant controllers (PIR) are used in this paper, since it is known which harmonic disturbance is to be expected in which vector plane.

The transfer function of the resonant component of the PIR controller is given in (20), where n is the order of harmonics that should be suppressed, $X(s)$ is the input and $Y(s)$ is the output of the resonant component of the PIR. Equation (20) can be transformed into (21). The complete PIR controller is shown in Fig. 8.

$$\frac{Y(s)}{X(s)} = \frac{K_{\mathrm{res}} \cdot s}{s^2 + (n\ \omega_{\mathrm{m}})^2} \tag{20}$$

$$Y(s) = K_{\mathrm{res}} \cdot X(s) \cdot s^{-1} - (n\ \omega_{\mathrm{m}})^2 \cdot Y(s) \cdot s^{-2} \tag{21}$$

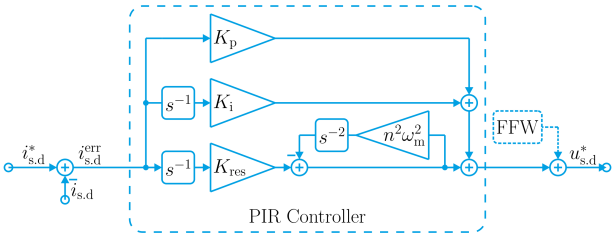

Fig. 8. PIR controller diagram (exemplarly for $i_{\mathrm{s.d}}$)

The resonant frequency $n\ \omega_{\mathrm{m}}$ of the PIR controllers are set to the 12^{th} harmonic frequency in dq plane and the 6^{th} harmonics frequency in $\mathrm{z_{dq}}$ plane. A PIR with two resonant components is used in $\mathrm{o_{12}}$ plane with resonant frequencies of the 3^{rd} and 9^{th} harmonics.

IV. The Drivetrain

The drivetrain has been designed as a retrofit replacement for a two-passenger, pure electric vehicle. The specifications of the drivetrain are given in Table I. The project required that the whole drivetrain fits into the space of only the machine of the previous drivetrain. Therefore a modular system, consisting of the machine, the inverter power stage and the control unit, has been designed to form a fully enclosed housing with water cooling to achieve high power density.

TABLE I. Drivetrain Specifications

Parameter	Variable	Value
Nominal mechanical power	$P_{\mathrm{m.N}}$	31.5 kW
Nominal torque	$T_{\mathrm{m.N}}$	100 Nm
Nominal rotational speed	$n_{\mathrm{m.N}}$	3000 rpm
Maximum rotational speed	$n_{\mathrm{m.max}}$	10000 rpm
Minimum battery voltage	$V_{\mathrm{batt.min}}$	80 V
Nominal battery voltage	$V_{\mathrm{batt.N}}$	108 V
Maximum battery voltage	$V_{\mathrm{batt.max}}$	120 V
Nominal phase voltage	$V_{\mathrm{ph.N}}$	70 V
Nominal phase current	$I_{\mathrm{ph.N}}$	100 A
Power factor	$\cos\varphi$	0.80
Number of pole pairs	p	3
Switching frequency	f_{sw}	50 kHz

The rotor of the machine is designed with a hollow shaft and a rotor mounted fan blade for air cooling. The blade of this cooling system goes through the inverter space, as shown in Fig. 9. This created a significant design challenge for the spacial distribution and cooling of the inverter. Both the rotor cooling system and the inverter spacial distribution led to patent pending ideas, details of which are given in [7] and [8].

A. The Inverter Power Stage and the Control Unit

The inverter consists of a power stage and a control unit, as shown in Fig. 10. The top, left, back isometric view of the inverter is given in Fig. 10-a with the control unit box open. The female plugs to connect the machine to the inverter, which save significant volume compared to a screw solution, can be seen in the top, front, left isometric view in Fig. 10-b.

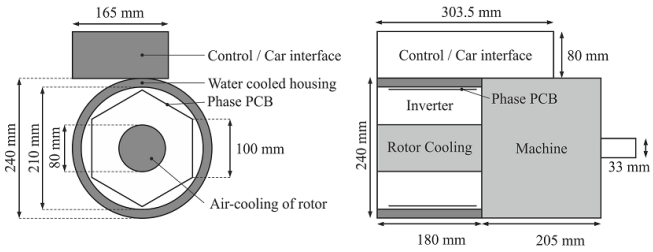

Fig. 9. The integrated drivetrain design

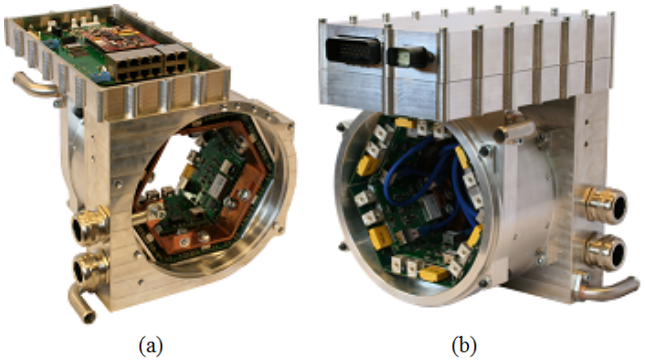

Fig. 10. The inverter: (a) Back isometric view, (b) Front isometric view

The power unit consists of six individual H bridges, mounted on the inner walls of a hexagonal water cooled housing. Due to the very restricted available mounting space, the H bridges are designed with DirectFET MOSFETs. This allows a very low mounting height as well as low stray inductances in the commutation path, thus allowing operation of the inverter close to the breakdown voltage of the MOSFETs.

Successful operation is verified up to a dc-link voltage of $V_{\mathrm{dc}} = 145\,\mathrm{V}$ using MOSFETs with a rated breakdown voltage of $V_{\mathrm{DS.BD}} = 150\,\mathrm{V}$. To further increase the power density, ceramic SMD capacitors are used in parallel to build up the dc link capacitor. A maximum inverter efficiency of $\eta = 97\,\%$ and power density of 5,4 kW/L is achieved.

The control unit includes the compact control system XCS2100 from the company AixControl. The control algorithm is run on a 150 MHz fixed-point DSP. 12 PWM signals for each half bridge are created by this system and processed by a Xiling CPLD to obtain the 24 gate signals for each MOSFET. Safety functions such as hardware overcurrent and overvoltage protection are also implemented by the CPLD. The control unit handles CAN communication with the vehicle. Further details of the inverter design can be found in [7].

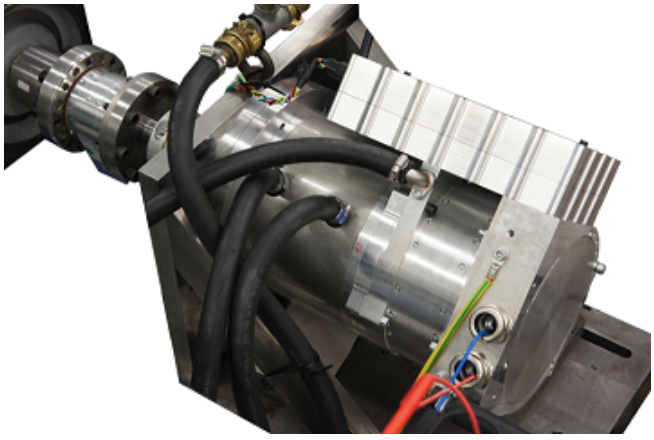

Fig. 11. The drivetrain installed on the testbench

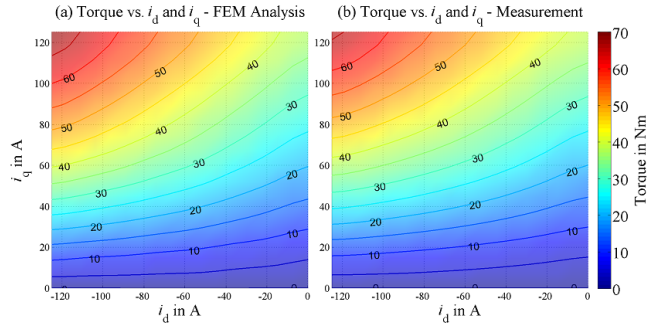

Fig. 12. Torque vs. $i_{s.d}$ and $i_{s.q}$: (a) FEM analysis, (b) measurements

B. The Machine

The IPMSM is a 3 pole-pair, distributed winding machine with V-shaped interior magnets. The stator has 36 slots, therefore 1 slot per phase per pole and 8 turns per slot. Reducing the slot pitch of the coil span allows to decrease the harmonic content. However, it is not implemented, since this effect is marginal in a six-phase winding system. In order to reduce the cogging torque, the stator is skewed by one tooth width. The machine has a very compact design, achieving a very high power density of 3 MW/m3. Further details of the machine design can be found in [8].

V. Simulations and Experimental Results

A. Machine Model Verification

1) Torque vs. $i_{s.d}$ and $i_{s.q}$: As the first step of the experimental model verification, the torque of the machine in FEM analysis and on the test bench have been compared. For this purpose, changing $i_{s.d}$ and $i_{s.q}$ values have been applied to the machine and the torque outputs have been measured. The results have shown that the FEM analysis torque calculations successfully represent the actual machine, as illustrated in Fig. 12.

2) Short Circuit Currents: The short circuit currents of machine models with various assumptions are compared to the measurements, in order to observe the impacts of these assumptions on the models. The results are given in stator oriented orthogonal space, since the current measurements do not have corresponding rotor angle data.

The assumption that the rotor field oriented orthogonal space dimensions are inductively decoupled leads to the assumption that the machine can be represented by the machine model, even when only the diagonal inverse inductance matrix is used instead of the complete inverse inductance matrix $\left[L_{s.dq}^{-1}\right]$. This assumption leads to inaccurate results, as can be seen by comparing (a) and (d) in Fig. 13.

The saturation has a very significant impact on the induced currents in z_{dq} plane as well as o_{12} plane, as the comparison between (b) and (d) in Fig. 13 illustrates. Simulations have also shown that the phase voltage of the machine "triples" at rated speed and torque, if the saturation is not taken into account. Therefore, saturation should not be neglected in order to obtain a representative machine model.

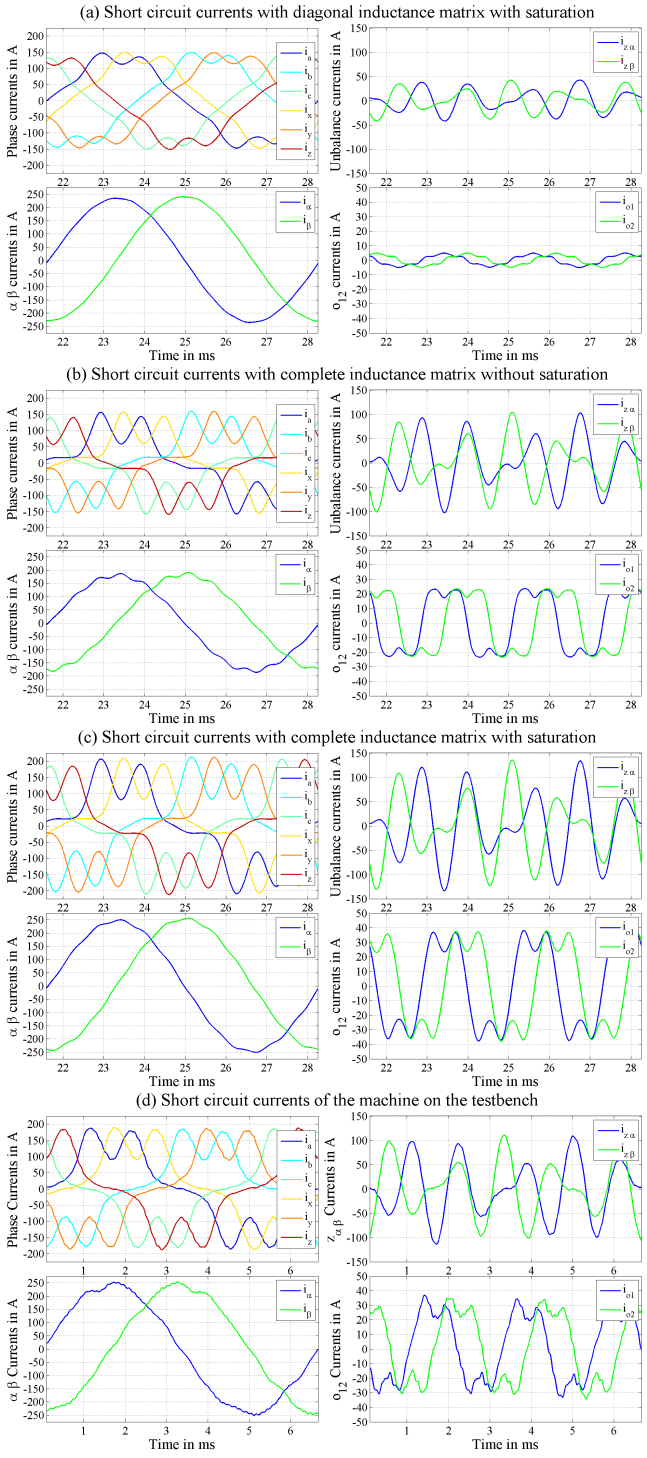

Fig. 13. Short circuit currents of machine models and the real machine

The IRTF based machine model is shown to adequately represent the machine as long as the rotor position and stator current dependencies of inductances and the magnet flux linkages as well as the inductive coupling between the rotor field oriented orthogonal space dimensions are taken into account, as shown in (c) and (d) in Fig. 13.

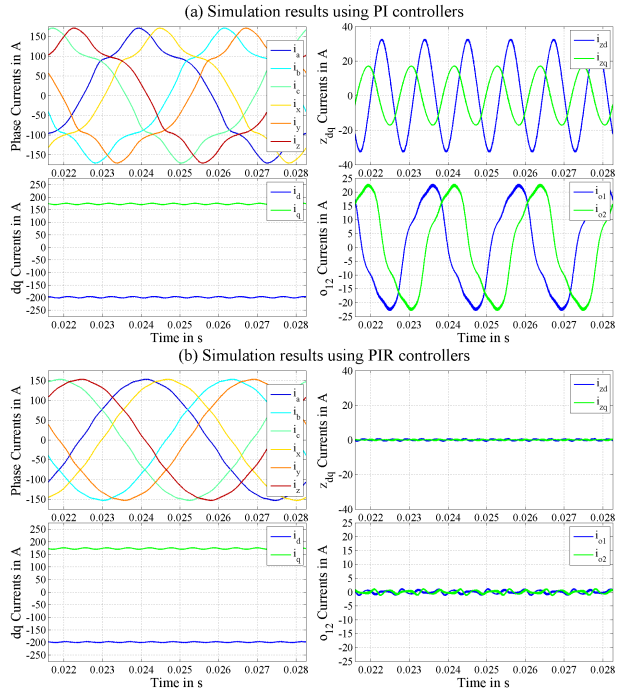

Fig. 14. Control simulations at rated speed and torque

B. Control Simulations

Control simulations have been carried out in MATLAB-Simulink. The controller and the machine models are implemented in Simulink, while the inverter is modeled using PLECS. The current sensor delay and discrete controller operation are implemented, while dead times in the inverter are not implemented.

The current waveforms of the machine at the rated operating point of rotor speed $n = 3000\,\mathrm{rpm}$ and torque $T_\mathrm{m} = 100\,\mathrm{Nm}$, using a PI controller and a PIR controller, respectively, are given in Fig. 14. The PIR controllers have successfully damped the harmonics, which could not be damped by the PI controllers.

C. Inverter and Machine Efficiencies

Efficiency maps have been obtained using a power analyzers on the dc link and the six phases of the machine to measure the electrical power at the input and output of the inverter; and using a torque-speed sensor to measure the mechanical power of the machine. 100 points of measurement have been taken for a varying mechanical torque output T_m between $5\,\mathrm{Nm}$ and $50\,\mathrm{Nm}$, and rotor speed n between $100\,\mathrm{rpm}$ and $1000\,\mathrm{rpm}$ to obtain the efficiency maps given in Fig. 15. An inverter efficiency of $97.1\,\%$ and a machine efficiency of $93.4\,\%$ have been achieved despite partial loading. The full operating range could not be achieved yet as of the date the paper has been written.

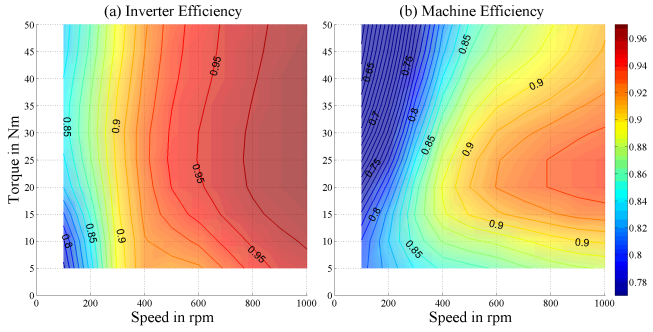

Fig. 15. Efficiency vs. speed and torque of (a) inverter and (b) machine

VI. Conclusion

A low voltage, high power drivetrain with an asymmetrical six phase, open-delta IPMSM and an H Bridge inverter has been designed for an electric vehicle. Field oriented modeling and control of such a system have been explored. The machine-based sources of unbalance and zero sequence current components have been investigated in further detail. It has been shown how these sources are related to the harmonics induced by the machine. Detailed simulations using machine models with verified FEM analysis are provided, along with efficiency measurements of the drivetrain.

VII. Acknowledgments

The results presented in this paper have been developed during the research project e-MoSys: ”Entwicklung und prototypische Umsetzung eines anfordergungsgerechten und modularen Antriebs- und Fahrwerkssystems fuer ein Elektrofahrzeug” (Development and prototype implementation of a specific and modular drive and suspension system for an electric vehicle) granted by the Ministry of Education and Research.

References

[1] R. De Doncker, W. J. D. Pulle, A. Veltman, *Advanced Electrical Drives - Analysis, Modeling, Control*, ISBN 978-94-007-0181-6, Springer, 2011.

[2] E. Levi, *Multiphase Electric Machines for Variable Speed Applications*, IEEE Transactions on Industrial, vol. 55, no. 5, pp.1893-1909, May 2008.

[3] E. Levi, R. Bojoi, F. Profumo, H. A. Toliyat and S. Williamson, *Multiphase Induction Motor Drives A Technology Status Review*, IET Electr. Power Appl., pp. 489-516, 2007.

[4] Y. Zhao, T. A. Lipo, *Space Vector PWM Control of Dual Three Phase Induction Machine Using Vector Space Decomposition*, IEEE Transactions on Industry Applications, vol. 31, no. 5, pp. 1100-1109, September/October 1995.

[5] Y. Hu, Z. Zhu, K. Liu, *Current Control for Dual Three-Phase Permanent Magnet Synchronous Motors Accounting for Current Unbalance and Harmonics*, IEEE Journal Of Emerging And Selected Topics In Power Electronics, Vol. 2, No. 2, June 2014.

[6] M. Neubert, S. Koschik, R.W. De Doncker, *Performance comparison of inverter and drive configurations with open-end and star-connected windings*, Power Electronics Conference (IPEC-Hiroshima 2014 - ECCE-ASIA), 2014.

[7] G. Engelmann, M. Kowal, R.W. De Doncker, *A Highly Integrated Drive Inverter using Directfets and Ceramic Dc-Link Capacitors for Open-End Winding Machines in Electric Vehicles*, Applied Power Electronics Conference and Exposition (APEC), Charlotte, NC, USA, 2015.

[8] T. Grosse, D. Franck, N. Conzelmann, D. Paul, C. Haenelt, A. Stapelmann, K. Hameyer *Compact Machine Design of an Integrated Multiphase VPMSM*, Electric Drives Production Conference (EDPC), Nuremberg, Germany, 2015